A Co-Simulation Methodology for the Design of Integrated Silicon Spin Qubits with their Control/Readout Cryo-CMOS Electronics

B. Gys*, R. Acharya*, S. Van Winckel, K. De Greve, G. Gielen*, F. Catthoor*

***Abstract*—Recent years have witnessed a steady growth in the achievable quantum systems due to advancements in qubit technology across several hardware platforms. Currently entering an era of noisy intermediate-scale quantum (NISQ) systems brings additional design challenges. In these systems, each individual qubit is accompanied by a substantial amount of classical CMOS circuitry for qubit instantiation, control and readout, which is to be integrated at the cryo temperature. This work presents a methodology for the co-design and co-simulation of silicon spin qubits in quantum dots, together with their associated cryo-CMOS circuitry, relying on an established spin qubit compact model. In addition, a detailed procedure is proposed for the integration of the model into a classical design flow, which is crucial for the usability of the model in practice. This is illustrated by simulating the readout of a qubit using a complete CMOS readout chip that behaves in a realistic, nonideal way. Bringing the design to a single simulation environment allows for the capture and analysis of effects that otherwise are not possible to simulate when considering the qubits and the cryo-CMOS circuitry separately. This opens up opportunities for more robust design in the future.**

***Index Terms*—Quantum computing, spin qubit, co-simulation, cryo-CMOS, qubit readout.**

I. Introduction

OVER the course of the past decade, significant progress in quantum computing research has been made by improving several qubit technologies and increasing the insight in the quantum computing stack. Along with the rising reliability of the systems comes the opportunity to expand their size and to take the next step in the research towards full-scale quantum computing. This places us currently at the beginning of an era during which noisy intermediate-scale quantum (NISQ) systems are being studied, with systems ranging in size from tens to thousands of qubits [1]. One of the more favorable technology platforms that offers the potential to build such systems is electron spin qubits in electrostatically confined quantum dots [2]–[4]. The good isolation from the surroundings in this implementation protects the fragile qubit state from quickly being destroyed by environmental noise [5]. The large maturity of the silicon manufacturing industry and the small qubit footprint are additional benefits, making this technology suited for upscaling the system size.

Irrespective of the physical implementation, each qubit requires a significant amount of classical CMOS electronics for its instantiation, control and readout, as shown in Fig. 1(a). In current experimental setups, these circuits are often placed outside the cryogenic cooling system and connected via numerous interconnects to the qubit devices. However, as the system size grows, this approach will become no longer feasible. Integration and operation of these classical circuits close to the qubit devices will be unavoidable, reducing the complexity of the system and increasing the reliability [6]–[8]. The design of classical CMOS control circuitry operated under cryogenic conditions, and its interaction with the qubit devices forms thus a fundamental part of quantum computer design research, receiving a rising interest [9], [10].

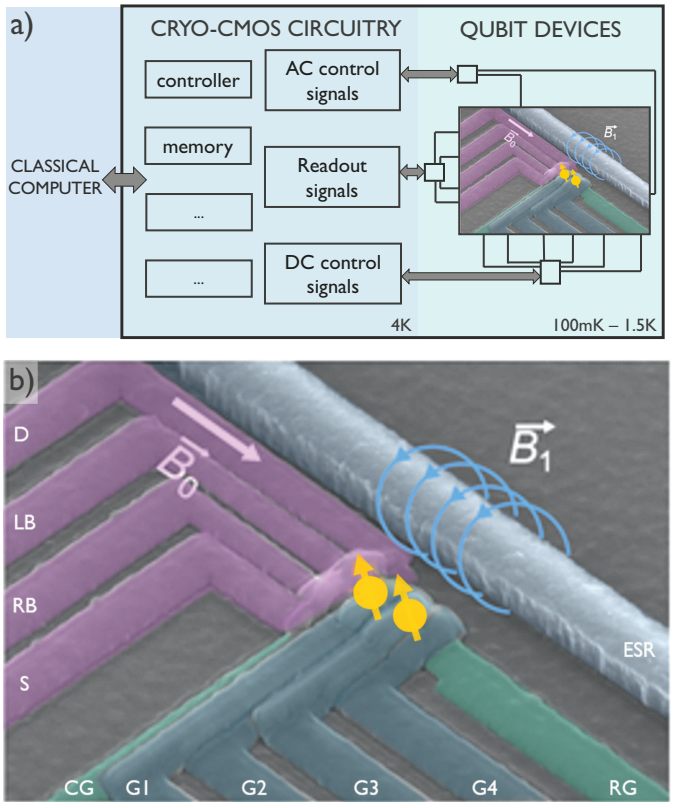

Fig. 1. (a) Schematic of a typical integrated quantum computing architecture, indicating the many control lines running from the cryo-CMOS circuitry to the qubit devices. The cryo-CMOS circuitry is required for qubit instantiation, control and readout. (b) Zoom of the SEM image showing a double quantum dot device containing two qubits (yellow), similar to the structure described in [11]. Each qubit state can be manipulated using a high-frequency ESR signal (light blue) and can be read out by a single-electron transistor (purple).

imec, Kapeldreef 75, Leuven, B-3001, Belgium, email: benjamin.gys@imec.be

*also with Department of Electrical Engineering (ESAT), KU Leuven, Kasteelpark Arenberg 44, Leuven, B-3001, Belgium

The qubit devices put very stringent requirements on the cryo-CMOS circuitry in terms of noise and power consumption [6], [12], resulting in the demand for a close co-design of the qubits and their classical electronics in order to capture all aspects of their interaction and the effects of nonidealities in the signals. It is to this end that a spin qubit circuit model has been developed to enable the co-simulation of spin qubits with their respective control and readout electronics in a common design environment [13]. This model is based on previous works indicating the suitability of well-established circuit simulator engines for the implementation of circuit-level quantum systems [14], [15]. The translation of the quantum system into an equivalent set of circuits representing its behavior allows for the use of a common design environment and therefore the analysis of the interaction between both subsystems and an increased usability. This can lead to a more robust design and opens up possibilities for the design of quantum microarchitectures.

This work extends the previously presented compact model [13] by the twofold novelties of (i) introducing a qubit design library, and (ii) proposing an implementation for the coupling of classical and quantum systems using nonideal control signals, making a co-simulation possible in practice. The introduction of a qubit library is required for the simulator engine to be able to handle the different needs of the electronic and the quantum subsystems in a single simulation. A correct modelling of the interface between the two subsystems, while making a trade-off between accuracy and simulation complexity, is crucial for the analysis of bidirectional and closed-loop effects. An example of such a bidirectional effect is the relation between ingoing and outgoing fields, while the reflection of signals back into the quantum system forms an example of a closed-loop effect. Whereas for the development of the original model [13] ideal signal sources were used, allowing the verification of the quantum behavior, in this paper a quantum system consisting of a spin qubit coupled to a readout resonator is interfaced to a full readout chip design [16], [17]. Although the chip has been developed for the readout of superconducting qubits, the requirements for spin and superconducting qubits are very similar when being read out using resonators [18], allowing the use of very similar CMOS circuitry. Note that spin qubits can typically be operated at higher temperatures than superconducting qubits, resulting in less strict requirements for the CMOS circuitry. Based on the illustrative system, we show in this paper that the proposed methodology can be used for the analysis of the effects of nonidealities in the transient signals and to derive subsequent design improvements to either of the subsystems, which is not possible when designing the subsystems in separate tools. Compared to other existing co-design methodologies aimed at the same goals [19], [20], a distinct advantage of the proposed methodology is the incorporation of bidirectional and closed-loop effects at the interface. This detailed implementation directly contributes to a better prediction of the effects of the control signals on the quantum system.

The remainder of this paper is structured as follows. In section II, the methodology of the compact model is shortly recapitulated for completeness, followed by a more detailed description of the translation into a qubit design library and of the methodology used for the coupling of classical and quantum systems. Section III discusses the simulation results generated based on the described illustrative system, showing the investigation of the impact of nonidealities. Finally, section IV concludes this work, summarizing the main achievements.

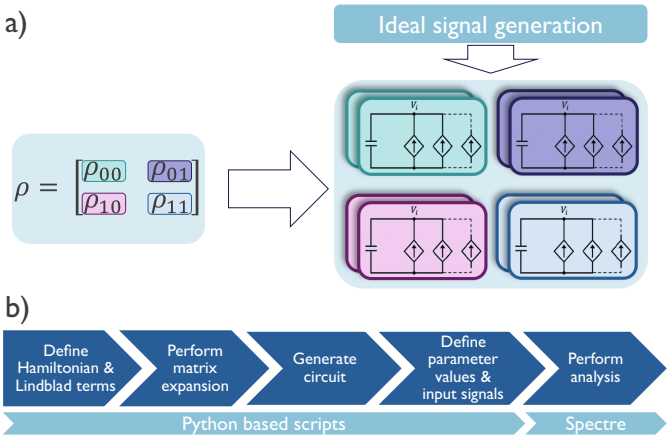

Fig. 2. Compact modelling methodology, figure adapted from [13]. (a) Schematic representation of the circuit generation representing the simulated quantum system from the system's density matrix. This circuit interfaces with classical electronics (chosen to be ideal for the verification of the model). (b) Modelling steps followed, relying on Python scripts, to generate a circuit representation as well as to start the co-simulation using the Spectre® engine.

II. Methodology

A. Spin Qubit Compact Model

This work builds upon a previously developed spin qubit compact model [13], that is based on an automated method for the conversion of the qubit's quantum behavior into an equivalent circuit representation. It is shortly recapitulated in this subsection for completeness. This modelling method is depicted in Fig. 2, together with a schematic flow of the steps for generation of the equivalent circuit from the quantum system's mathematical description.

The unitary time evolution of a quantum system can be described using the Liouville-von Neumann equation [21]:

$$\dot{\rho}(t) = -\frac{i}{\hbar}(H\rho(t) - \rho(t)H). \tag{1}$$

In this equation, $\hbar$ is the reduced Planck constant (= $h/2\pi$) and H is the Hamiltonian of the system, which describes its energy and governs the time evolution. $\rho(t)$ is called the density matrix at time t and represents the state of an open quantum system, which is a statistical mixture of pure states. It is calculated as:

$$\rho = \sum_i p_i \left|\psi_i\right\rangle \left\langle\psi_i\right|, \tag{2}$$

where $|\psi_i\rangle$ are the pure state vectors of size n, and $p_i = \langle\psi_i|\,\rho\,|\psi_i\rangle$ are the respective probabilities of finding the system in this state. If the open quantum system is interacting with an external environment, the Liouville-von Neumann equation (1) needs to be adapted to the Master equation in Lindblad form [22]:

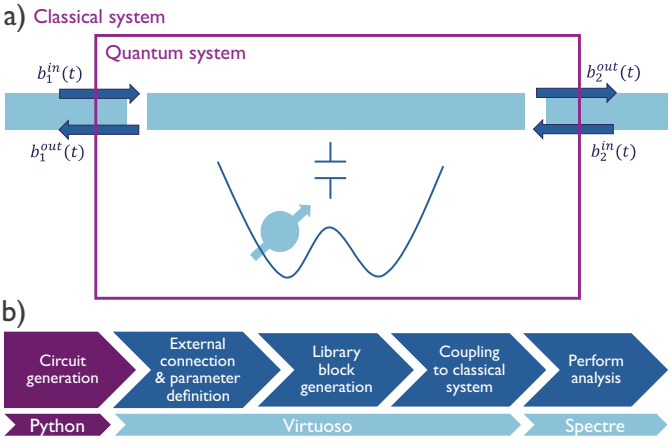

Fig. 3. Extended and optimised modelling methodology. (a) Schematic representation of the structural coupling between the quantum and classical subsystems, respectively inside and outside the purple box. The interface between the subsystems is defined by the fields $b_i^{in}(t)$ and $b_i^{out}(t)$, calculated using quantum input-output theory. (b) New flow of the steps followed for the construction of a qubit design library block and subsequent full-system analysis. The starting point of this design flow is based on the original approach of Fig. 2, indicated in purple; the extensions are drawn in blue.

$$\dot{\rho}(t) = -\frac{i}{\hbar}[H, \rho(t)] + \sum_i \gamma_i (L_i \rho(t) L_i^\dagger - \frac{1}{2}\{L_i^\dagger L_i, \rho(t)\}). \quad (3)$$

In this extended equation, the Lindblad operators L_i describe the channels of interaction with the external environment that result in relaxation and dephasing of the system [23]. The rates at which these respective effects take place are given by γ_i.

The notations in eq. (1) and (3) are representing a set of n^2 coupled, complex differential equations that can be split into the real and imaginary parts of each equation and reduced to $(n^2 - 1)$ real-valued equations by taking advantage of the properties of density matrices. These reduced notations have the following form:

$$\dot{\lambda}_i(t) = \sum_{j=1}^{n^2-1} G_{ij} \lambda_j(t), \quad (4)$$

where λ_i are real functions. Note that this expression has the exact form of Kirchhoff's current law describing the voltage across a capacitor, charged by a number of voltage-dependent current sources. Consequently, the quantum system can be interpreted, mapped and calculated in terms of electronic components, employing the optimised circuit simulator engines widely used for electronic design, as shown in Fig. 2(a). This allows for the seamless co-simulation and co-design with classical electronics.

Fig. 2(b) shows the complete automated flow for the circuit generation and simulation, starting from the construction of the Hamiltonian which defines the simulated system. The Hamiltonian is then converted into a reduced set of subcircuits based on the methodology described above. The parametric approach up to this step allows for efficient and flexible code. Before the simulation is launched, numerical values are assigned to the parameters and the input signals are defined. This flow is now extended in the context of this work.

B. Qubit Design Library

In the extended design flow, as depicted in Fig. 3(b), the one-time definition of the system's structure still happens based on the previous Python scripts. The generated circuits are now written as a subcircuit in a single Spectre® file that is part of a design library. By hiding the internals of the quantum system behind the definition of a subcircuit, with only the relevant connections and variables for setting physical parameters available to the outside world, abstraction is introduced and the usability of the model is greatly increased. In addition, the model is opened up to a wider range of designers, now only requiring a very basic knowledge of the quantum system during the design of the cryo-CMOS circuitry. Finally, the library structure also allows for the easy inclusion of additional blocks that are useful during design but might be based on different modelling methods, such as a Verilog® single-electron transistor (SET) model for sensing charges during qubit instantiation or qubit readout. These additional blocks offer the possibility of studying additional aspects of the system, like qubit instantiation with DC-gates for instance.

The introduction of the library not only increases the usability, but also entails the crucial task of determining the accuracy settings for the subcircuit, making a co-simulation possible in practice. Since the quantum and classical subsystems are of a fundamentally different nature, they also have different requirements concerning simulation accuracy. This has to be taken into account when making the trade-off with simulation time. While a global maximum simulation time step needs to be determined based on this trade-off, the usage of a library block allows to tighten the accuracies for this subcircuit only, minimising the impact on the overall simulation time. In Cadence®, this is done by setting the scoped user options (reltol, vabstol, iabstol). These options will impose stricter conditions for convergence on the selected nodes and leave the other nodes unaffected. This issue posed no problem when developing the compact model [13], since merely very basic circuitry was used for the generation of ideal control signals, but it becomes considerably more important when the size of the classical system increases with respect to the quantum system. An explosion of the simulation time is avoided by using the library models.

C. Coupling Classical and Quantum Systems

Once nonidealities are included in the analysis, the interface between the classical and quantum subsystems needs to be considered carefully, to determine whether an effect can be neglected or not. The illustrative quantum system used in this work consists of a single electron spin in a double quantum dot that is capacitively coupled to a two-port resonator for dispersive state readout [13], [24]. These two ports form the only connection to the outside world, as depicted in Fig. 3(a). A static external magnetic field is applied to induce Zeeman splitting and to define the two energy levels that make up the qubit [5]. The qubit state can be manipulated based on the principle of electron spin resonance (ESR) [25]. To identify the effects of nonidealities in the signal probing the readout resonator, all channels of relaxation and dephasing in the

quantum system are neglected, except for the relaxation of the resonator caused by power leaking out at its ports. This channel is required for making the connection with the readout chip and to avoid the buildup of power inside the resonator. This results in the following mathematical description:

$$H = H_S + H_R, \tag{5}$$

$$\text{with } H_S = h\gamma_E B_0 \sigma_z + h\gamma_E B_{ac}(t)\sigma_x, \tag{6}$$

$$H_R = hV_t\sigma_{cz} + hf_{cav}a^\dagger a + h(a+a^\dagger)(V_{c,1}(t)+V_{c,2}(t)) + H_I. \tag{7}$$

The first term (6) of the Hamiltonian accounts for the spin, while the second term (7) describes the readout resonator coupled to the spin state. In the first term (6), γ_E is the gyromagnetic ratio of an electron ($\sim$ 28GHz/T), B_0 is the static magnetic field, B_{ac} is the high-frequency magnetic field induced by the ESR line and σ_z and σ_x are the Pauli matrices. In the second term (7), V_t is the tunnel coupling between the two quantum dots, σ_{cz} is the Pauli-Z matrix for the charge state of the electron, f_{cav} is the resonance frequency of the resonator, a and $a^\dagger$ are the respective annihilation and creation operators, $V_{c,1}$ and $V_{c,2}$ account for the input signals applied to the two ports of the resonator and, finally, H_I describes the interaction between the electron charge state and the resonator. This Hamiltonian (5) is combined in the Master Equation (3) with the two Lindblad terms that correspond to the relaxation of the resonator through its two ports:

$$L_1 = L_2 = \kappa(a\rho a^\dagger - \frac{1}{2}\{a^\dagger a, \rho\}), \tag{8}$$

for which the relaxation rates $\kappa_1 = \kappa_2 = \kappa$ are equal. The Hamiltonian governs all internals of the quantum system, meaning that noise in signals applied to the resonator ports and back-action effects from the classical CMOS circuitry can affect the qubit through the resonator, provided that they are presented correctly to the quantum system.

This task of interfacing the classical and quantum subsystems requires classical input-output theory to be combined with quantum theory. It can be modelled in terms of the incoming and outgoing fields, as depicted in the schematic of Fig. 3(a). The fields at port i are related as:

$$b_i^{out}(t) = b_i^{in}(t) + \sqrt{\kappa_i}a(t), \tag{9}$$

where κ_i are again the relaxation rates. The outgoing fields $b_1^{out}(t)$ and $b_2^{out}(t)$ are calculated internally inside the qubit library block, as expectation values, according to the following operator [26]:

$$\hat{V}(t) = \sqrt{\frac{Z_0}{2}}\frac{1}{\sqrt{2\pi}}\int d\omega\sqrt{\hbar\omega}(\hat{A}_\omega e^{-i\omega t} + \hat{A}_\omega^\dagger e^{i\omega t}), \tag{10}$$

and made available as outputs of the qubit block. $\hat{A}_\omega$ is the field amplitude operator at angular frequency ω. Note that the classical output voltages are thus proportional to the outgoing photon flux. When only considering one frequency component, this expression can be reduced to:

$$\hat{V}(t) = \sqrt{\frac{Z_0\hbar\omega}{2}}(\hat{A}_\omega e^{-i\omega t} + \hat{A}_\omega^\dagger e^{i\omega t}). \tag{11}$$

The incoming fields $b_1^{in}(t)$ and $b_2^{in}(t)$ can be calculated based on the classical voltages and are presented as an input to the quantum system through the voltages $V_{c,1}(t)$ and $V_{c,2}(t)$. These time-dependent voltages are generated by the classical CMOS circuitry during the simulation. At the resonator input port 1, the field is dominated by the probing signal put on the line connected to this port by the classical CMOS circuitry. Consequently, $b_1^{out}(t)$ can be neglected. At the output port 2, this is not the case because the line connected to this port is not driven.

This approach makes a design trade-off possible between accuracy and simulation time. In this case incorporating strong

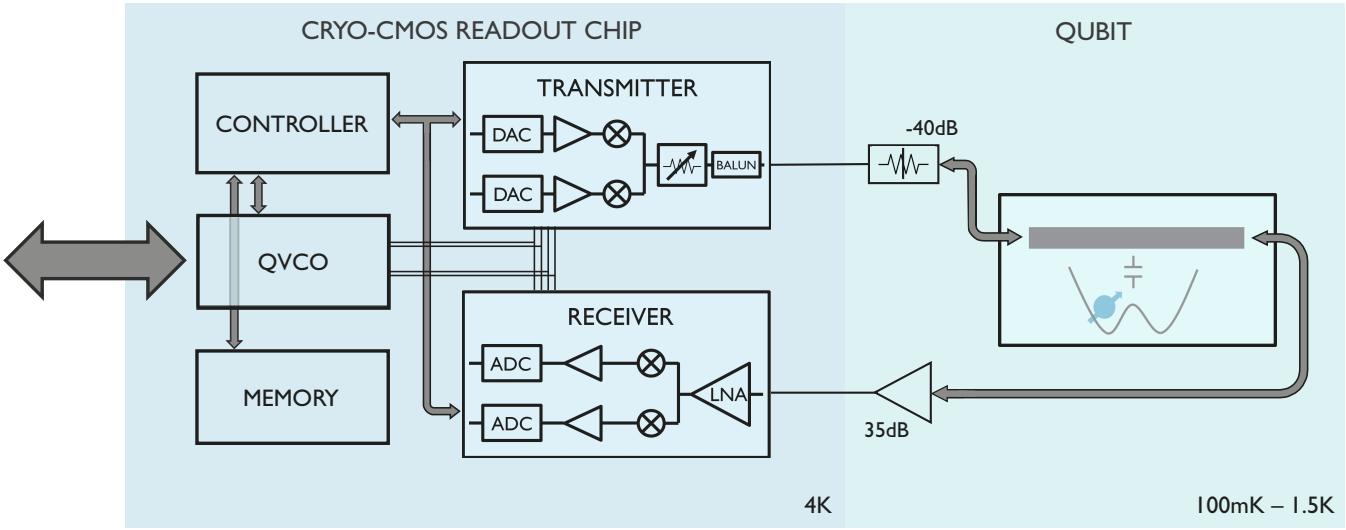

Fig. 4. Schematic of the complete simulated system, showing all interconnectivity. The transmitter generates a probing pulse which is attenuated by cryo-CMOS circuitry close to the qubit. This pulse drives the readout resonator inside the quantum system. The dispersive readout signal that leaks out of the right resonator port and that contains the qubit state information is processed by the receiver after initial amplification close to the qubit.

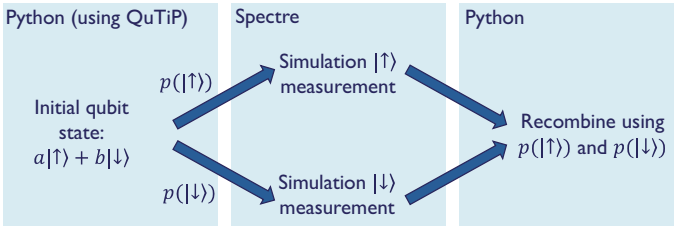

Fig. 5. Simulation approach for the measurement of a qubit in a superposition state by splitting the simulation into multiple measurement paths. The collapse is handled by Python code, which is better suited for this task. Next, the time evolution for each of the different paths is simulated in Spectre®. Finally, the simulation results are recombined in Python, and can later be used for applying more operations on the qubit.

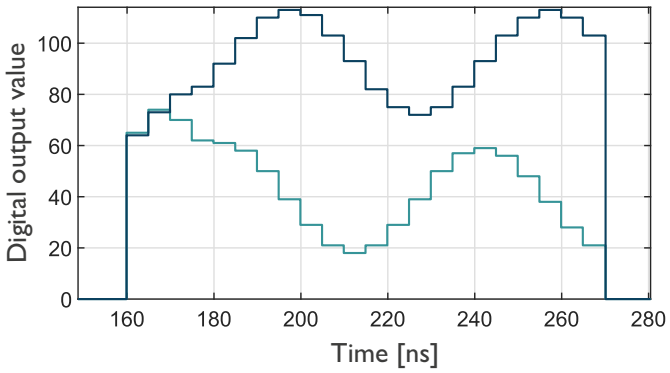

Fig. 6. Typical processed output. The high-frequency readout signal coming from the qubit is amplified, demodulated into I and Q components and digitized into 7-bit words at a speed of 200MS/s.

effects such as the reflected signals due to nonperfect matching, but neglecting weaker effects such as the shot noise due to the statistical process of photons leaking out of the resonator. The designer can make a balance appropriate to the investigated system by choosing the effects incorporated into the Hamiltonian when creating a new library block. The relative importance of specific effects, on the simulated system as well as on the simulation time, can be investigated by making different versions of library blocks and exploring the impact of the different effects. In a realistic design scenario, it is desired to include additional effects causing qubit decoherence as well. Adding these effects has shown to only cause a slight increase in simulation time. For most simulated systems this increase is around 10%, and it never comes close to 100%.

III. Results

In this section the benefits of the proposed methodology over a split design approach are demonstrated, based on the simulations of the example system consisting of a spin qubit coupled to a readout resonator that is probed and read out by cryo-CMOS circuitry that is specifically designed for this purpose (Fig. 4) [16]. First, the complete simulated system is described in detail. Then the tight, closed-loop effects of the interaction between the classical and quantum subsystems are discussed, which form the aim of the methodology. For the specific system under analysis, these are the tuning of the readout chip to the needs of the qubit, the effects of nonidealities

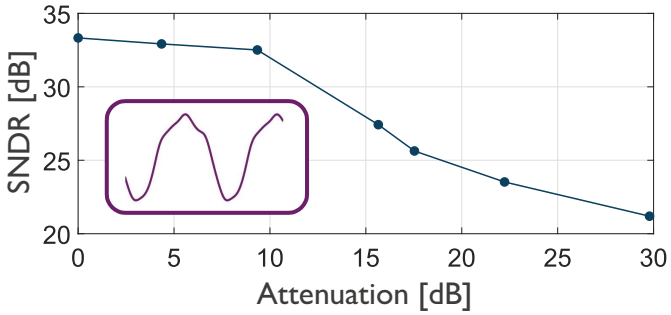

Fig. 7. Simulated SNDR of the transmitter output signal as a function of the attenuation setting inside the transmitter block of Fig. 4. For the higher settings the output actually starts to deform, causing the SNDR to drop. The insert illustrates this deviation of the transient waveform from the expected sinusoidal signal.

in the applied signals and the effects of nonperfect matching between the lines connecting the quantum subsystem and the classical circuitry closest to the quantum subsystem. Note that these effects differ from system to system, but that the proposed methodology can be applied in exactly the same way to other systems, for example to study cryo-CMOS circuitry generating nonideal ESR signals for qubit operations.

The proposed methodology is aimed to be part of a larger framework for studying qubit evolution over multiple consecutive operations. Some quantum behavior, like the collapse of the wave function that is relevant for the illustrative system, is not well suited to be simulated in Spectre® due to discontinuities in the signals. Since the cryo-CMOS circuitry has no influence on this phenomenon, there is also no need to simulate this in Spectre®. Instead it is handled by Python code, using the QuTiP optimised quantum toolbox [27]. For each possible measurement outcome a separate Spectre® simulation is started, of which the results are then recombined in Python using their respective measurement probabilities (Fig. 5). Note that this approach also does allow the study of quantum effects that are influenced by the cryo-CMOS circuitry, like the decoherence that happens during the measurement process simulated in Spectre®.

A. Simulated System for State Readout

Fig. 4 shows the schematic representation of the complete simulated system, consisting of the readout circuitry coupled to the qubit-resonator quantum system. A detailed description of the quantum subsystem was given in section II.C, since it is closely linked to the implementation of the interface. The readout chip has been designed previously in a 28-nm CMOS technology and consists of a low-power design including internal memory, controller, quadrature VCO, transmitter and receiver [17]. The DACs, ADCs and digital components operate at 7-bit 200MS/s. For the purpose of this paper the transmitter and receiver are of the largest importance since these are the blocks that generate and process the signals interacting with the quantum system. The chip has been designed to operate at a temperature of 4K, together with simple amplification and attenuation circuits closer to the qubit devices, which are chosen to be ideal circuits for the purpose of

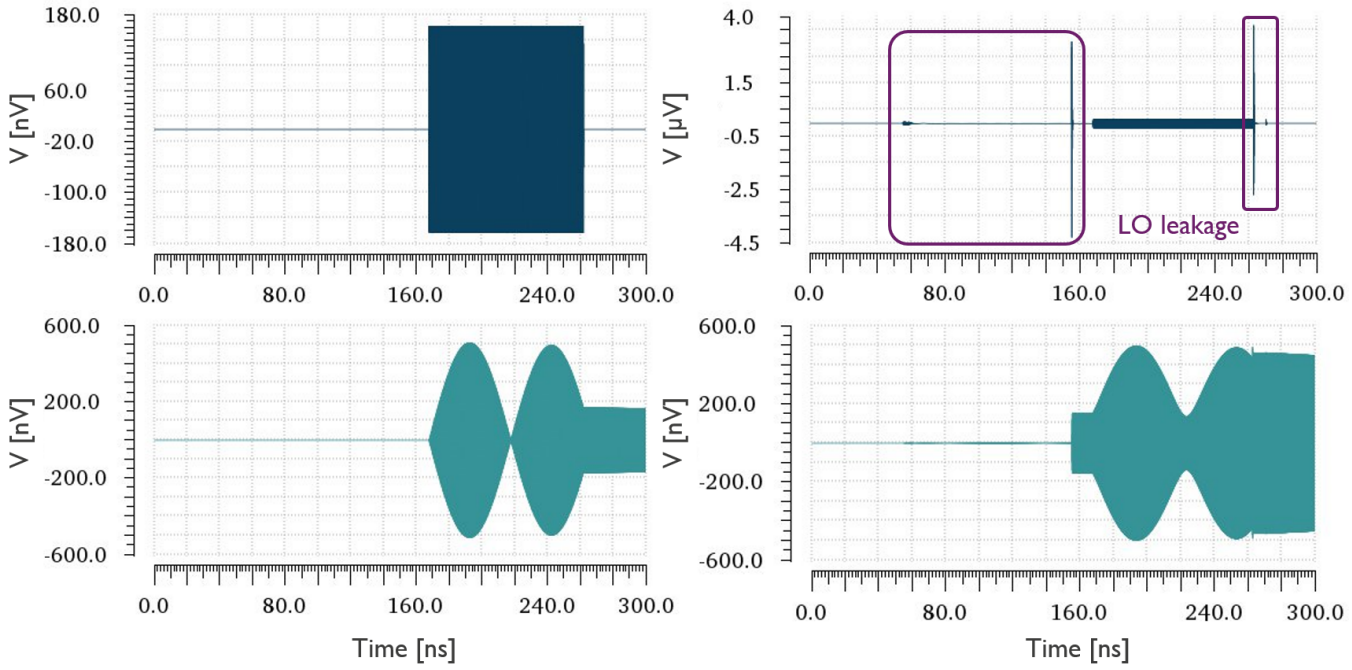

Fig. 8. Comparison between the ideal probing pulse and the pulse generated by the readout chip (top) and their resulting direct readout signals (bottom). The readout pulse generated by the chip (top right) contains undesired peaks that are significantly larger in amplitude than the readout pulse itself. This results in a deformation of the readout signal (bottom right).

this analysis. The total complexity of the cryo-CMOS circuitry is >100k transistors.

For achieving a very low power consumption, the chip is operated in a duty-cycled manner consisting of 3 modes: an idle, biasing and readout mode. When no readout takes place, the chip can be idle, resulting in a power dissipation that practically equals zero. This implies that the readout phase needs to be preceded by a biasing phase for powering up the circuits. During the readout mode, a probing signal matching the frequencies of the quantum system is generated by the transmitter. This signal shifts slightly in phase and frequency depending on the qubit state and is processed by the receiver. Fig. 6 plots a typical processed readout signal after amplification, demodulation and digitization. The phase of this dispersive readout signal is then used to distinguish the state of the qubit.

B. Tuning the Readout Chip to the Needs of the Qubit

A first important consideration when designing the coupling of the two subsystems is the matching of specifications, presenting the designer with some important decisions. The choice for the amplitude and frequency of the readout pulse requires careful consideration, since these choices have a considerable influence on the readout signal. This gives the designer the opportunity to tune the achievable resolutions. However, note that this also implies that undesired variations in the signal characteristics may reduce the accuracy. In addition, the designer has to keep other constraints in mind such as the fact that larger-scale systems will need to rely on frequency multiplexing and that the chip is designed to work with supplementary circuitry closer to the qubits. A probing signal producing too much power could also lead to transitions between the qubit states.

In this context, the proposed methodology can offer valuable contributions when tuning the readout chip and determining design choices for (future) additional circuitry. The chip itself has limited ranges for frequency, amplification and attenuation. In addition, pushing the chip to the edges of its range can cause the signals to deform. A tunnel coupling V_t corresponding to a frequency of 7.05GHz for the charge state of the qubit and a resonator frequency $f_{cav} = 6.9$GHz were chosen, falling in the 6.5-8.1GHz range of the chip. The pulse generated by the chip will approach this frequency of 6.9GHz, but unlike in ideal simulations a perfect sine wave will not be achieved. Fig. 7 shows the simulated SNDR of the transmitter output signal as a function of the attenuation setting inside the transmitter block. For the higher attenuation settings, the generated signal starts to deform, and influences the qubit readout signal. However, a considerable amount of attenuation (55-60dB) is required after the mixer of the transmitter for achieving the power levels that are typically used for probing spin qubits. Here, a power of -123dBm is targeted. The methodology allows to make the trade-off between the deformation of the signal and the amount of attenuation in the transmitter itself. An attenuation of ~15dB was chosen inside the transmitter, which is just above the point where the deformation of the signal starts to become the dominant effect, as shown by Fig. 7. This results in a requirement of at least 40dB of attenuation in the circuitry close to the qubit, compared to 30dB in [28]. For the amplification of the readout signal, the receiver offers a larger margin, resulting in a choice of 35dB amplification close to the qubit (Fig. 4). These considerations can be taken

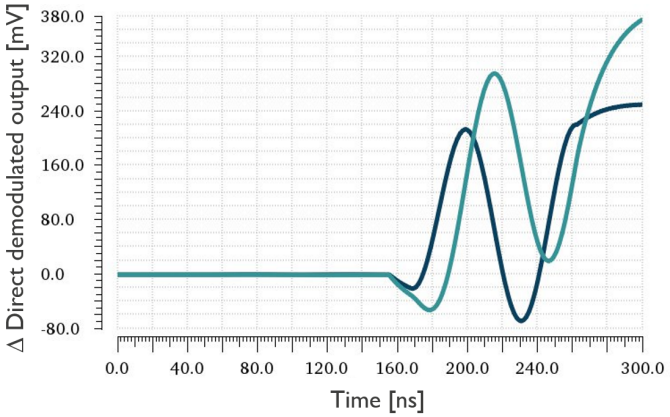

Fig. 9. Difference in I and Q components between the ideal readout signal and the one resulting from the probing pulse actually generated by the chip. The analytically calculated I and Q components of the chip readout signal may differ from the ones generated in the chip itself due to further nonidealities in the receiver circuitry.

into account to improve the chip design in the future or to optimize it for usage with spin qubits.

C. Effects of Nonidealities

Besides the variations in amplitude and frequency described in the previous subsection, realistic probing pulses may contain other nonidealities such as the deformations of the pulse shape, undesired frequency components, etc. These effects are not linked to design choices but find their origin in limitations of the performance of the CMOS circuitry. Based on the proposed methodology, the direct effects of these nonidealities on the qubit on the one hand and on the readout signal on the other hand can easily be analysed.

The analysis performed for the investigated system brings the insight that there is one very dominant effect, namely a signal leakage that is present at the transmitter output during the biasing phase of the readout chip. This leakage is originating in the local oscillator and causes photons to leak into the readout resonator. Fig. 8 shows the LO leakage, which is significantly larger in amplitude than the probing pulse itself (e.g. -94.4dBm for the chosen pulse strength of -123dBm), together with its effects on the readout signal. This is compared to the case of an ideal probing pulse. Tracking the evolution of the qubit confirms the expectation that the leakage is still short enough in time, low enough in power and far enough in the frequency spectrum to have a negligible influence on the qubit state. However, the effects on the readout signal are not to be neglected. The main result is a phase shift of the readout signal, as can be seen by calculating the difference between the demodulated I and Q components from the ideal readout signal and the readout signal resulting from the probing pulse generated by the chip (Fig. 9). Fortunately, the leakage remains unchanged for consequent simulated measurements with the same chip settings, meaning that the resulting phase shift can be taken into account when interpreting the final readout result. For the studied case, the leakage results in a phase error of 2.135 rad.

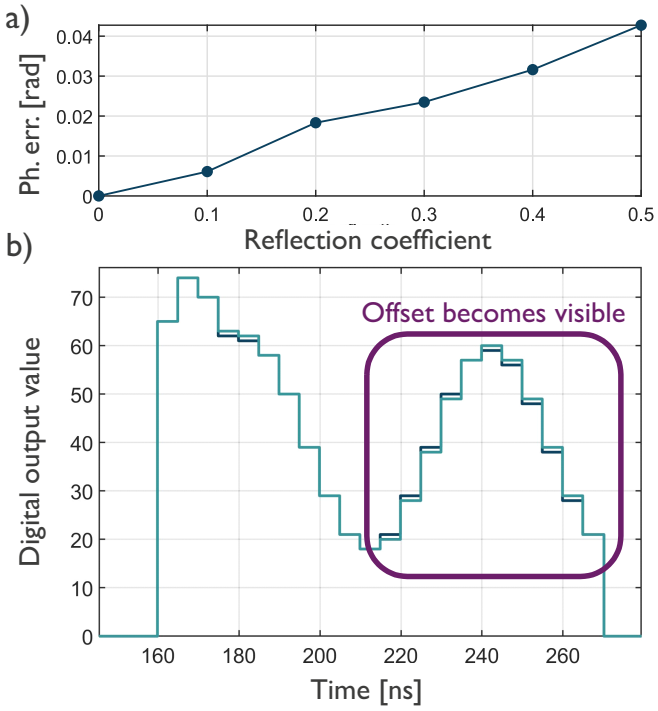

Fig. 10. (a) Simulated phase error of the direct readout signal caused by its reflection back into the resonator due to nonperfect matching of the lines connecting the quantum subsystem and the classical circuitry closest to the quantum subsystem. An arbitrary phase shift is chosen for the reflected signal and the errors are calculated at the end of the probing pulse. (b) Difference in I-component of the digital demodulated output between the case with perfect matching (blue) and the case with 30% reflection at the receiver side (green). During the first half of the pulse the errors still appear as random, while in the second half of the signal a structural offset becomes visible.

The presented methodology offers here the valuable contribution of confirming that the LO leakage in the current chip design can be handled. In addition to the oscillator leakage, there are some small variations in the probing pulse frequency as well. However, the effects of these variations are limited to a relatively small drop in the resonator signal power. Note that due to the dispersive readout technique, the effects of nonidealities in the readout pulse on the qubit state are limited. Signals generated by other cryo-CMOS circuits and that may contain nonidealities, such as the ESR signal, can have a far greater influence if they directly interact with the qubit itself. These signals can be analysed in the exact same manner.

D. Nonperfect Matching

If the lines connecting the CMOS circuitry to the qubit are not matched perfectly, the signal can partly be reflected back into the readout resonator at port 2, again causing a disruption from the ideal case. The amount of phase shift acquired by the reflected signal is dependent on the physical specifications of the transmission lines. For Fig. 10, which shows the simulated error introduced by the reflected signal, an arbitrary shift is chosen. This shift is fixed for all subsequent simulations. Unlike the error introduced by the LO leakage, the error due to nonperfect matching starts out small and accumulates over time. Fig. 9(a) plots the simulated error on the readout signal at

the end of the probing pulse for different amounts of reflection. As can be seen from the figure, the error grows linearly with the amount of reflected signal.

Since this error is rather small, the readout signal is mostly mapped to the correct digital output value by the readout chip. Within the duration of the probing pulse, only an occasional error occurs for the lower amounts of reflection. Due to the accumulation of the error, the frequency of incorrectly digitized output values increases, eventually forming an offset if the length of the probing pulse or the amount of reflection is increased. Fig. 9(b) compares the I-component from the digital output for the case with perfect matching to the case where 30% of the readout signal is reflected back into the readout resonator. This is the point where the offset in the digital output starts to become visible during the second half of the probing pulse.

These considerations are useful for the circuit designer during the design process of the cryo-CMOS circuitry close to the qubit.

E. Analysis of the Simulation Time

The simulation times for all simulations described in the previous sections for the illustrative system are ranging from one hour for the least complex simulations to 24 hours for the most complex ones, which are those incorporating the most closed-loop effects between the quantum and the classical subsystems. All simulations are executed using a single Intel® Xeon® E5-2667 v4 CPU with a maximum frequency of 3.20 GHz. These times are very reasonable for the targeted types of simulations.

Still, for future circuit studies with more qubits, the complexity will grow exponentially. No classical simulation approach for a quantum system is scalable. During future design, however, it may be useful to study quantum systems larger than the illustrative system described in this paper. We suggest two options for decreasing the simulation time when necessary. Firstly, approximations can be made in the quantum mechanical system. One example is applying the rotating wave approximation. Note that some of these simplifications may bring a decrease in accuracy. A second suggestion could be to use a CPU with more cores, increasing the level of parallelism. Using this second approach we have found that the number of qubits that can be studied in a single simulation while still maintaining reasonable simulation times is around six to seven qubits, depending on the complexity of the complete system. This number is comparable to other complete Master equation simulations in literature [29], while our approach additionally incorporates the circuit nonidealities impact.

F. Discussion

The behavior of the model in the ideal case has previously been verified against theory and other quantum simulation tools [13]. When simulating using the complete cryo-CMOS chip, we see the same state-dependent frequency and phase shifts as found in literature and previous ideal simulations. The obtained readout signal is correctly downconverted and digitized. In addition, the nonideal effects found during the design of the chip are affecting the quantum system as expected, namely by creating the deviations in the pulse shapes expected from theory, which ultimately translate to a phase error of the signal containing the qubit state information. Furthermore, when extrapolating the nonidealities to negligible values, the behavior of the system again approaches the ideal situation. This shows the correctness of the presented simulation methodology. However, the quantitative validation of the results will require detailed model calibration based on future hardware experiments.

IV. Conclusion

In this work a simulation methodology has been presented for the co-design of qubits with their classical cryo-CMOS control and readout electronics. The methodology is particularly aimed at connecting the quantum and classical subsystems, making a balance between simulation complexity and accuracy. This modelling is able to capture closed-loop effects of the interaction between the subsystems that cannot be studied in a split design approach, and is therefore better suited to assess the effects that nonidealities in the control signals generated by the CMOS circuitry have on the qubits. The practical usability of the modelling and simulation approach is illustrated by the study of a quantum system consisting of a spin qubit in a double silicon quantum dot and readout resonator that is coupled to a full readout circuit, generating all the necessary signals for the probing of the readout resonator and processing the qubit readout signal into a digital output. Three examples of tight interactions for this specific system have been highlighted. The same approach can be applied to other systems as well, opening up possibilities for the future design of NISQ systems and the formulation of design specifications for their classical control and readout circuitry.

Acknowledgements

The authors would like to thank the imec cryo-CMOS and spin qubit device teams for their contribution to this paper. Special thanks go to F. A. Mohiyaddin for his valuable support and to L. Burgelman for providing additional insights.

References

[1] J. Preskill, "Quantum computing in the nisq era and beyond," *Quantum*, vol. 2, p. 79, Aug 2018.

[2] M. Veldhorst et al., "An addressable quantum dot qubit with fault-tolerant control-fidelity," *Nature Nanotechnology*, vol. 9, no. 12, pp. 981–985, 2014.

[3] L. M. K. Vandersypen et al., "Interfacing spin qubits in quantum dots and donors—hot, dense, and coherent," *npj Quantum Information*, vol. 3, sep 2017.

[4] N. I. Dumoulin Stuyck et al., "Uniform spin qubit devices with tunable coupling in an all-silicon 300 mm integrated process," in *2021 Symposium on VLSI Circuits*, pp. 1–2, 2021.

[5] G. Burkard et al., "Semiconductor spin qubits." arXiv, 10.48550/arxiv.2112.08863, 2021.

[6] M. Mehrpoo et al., "Benefits and challenges of designing cryogenic cmos rf circuits for quantum computers," in *2019 IEEE International Symposium on Circuits and Systems (ISCAS)*, pp. 1–5, 2019.

[7] J. P. G. van Dijk et al., "The electronic interface for quantum processors." arXiv, 10.48550/arXiv.1811.01693, 2018.

[8] J. Craninckx et al., "Cmos cryo-electronics for quantum computing," in *2020 IEEE International Electron Devices Meeting (IEDM)*, pp. 25.1.1–25.1.4, 2020.

[9] B. Prabowo et al., "13.3 a 6-to-8ghz 0.17mw/qubit cryo-cmos receiver for multiple spin qubit readout in 40nm cmos technology," in *2021 IEEE International Solid- State Circuits Conference (ISSCC)*, vol. 64, pp. 212–214, 2021.

[10] B. Patra et al., "19.1 a scalable cryo-cmos 2-to-20ghz digitally intensive controller for 4×32 frequency multiplexed spin qubits/transmons in 22nm finfet technology for quantum computers," in *2020 IEEE International Solid- State Circuits Conference - (ISSCC)*, pp. 304–306, 2020.

[11] F. A. Mohiyaddin et al., "Multiphysics simulation & design of silicon quantum dot qubit devices," in *2019 IEEE International Electron Devices Meeting (IEDM)*, pp. 39.5.1–39.5.4, 2019.

[12] J. P. G. van Dijk et al., "Impact of classical control electronics on qubit fidelity," *Physical Review Applied*, vol. 12, oct 2019.

[13] B. Gys et al., "Circuit model for the efficient co-simulation of spin qubits and their control amp; readout circuitry," in *ESSCIRC 2021 - IEEE 47th European Solid State Circuits Conference (ESSCIRC)*, pp. 63–66, 2021.

[14] W. R. Zimmerman, "Time domain solutions to partial differential equations using spice," *IEEE Transactions on Education*, vol. 39, no. 4, pp. 563–573, 1996.

[15] R. Acharya et al., "Circuit models for the co-simulation of superconducting quantum computing systems," in *2021 Design, Automation Test in Europe Conference Exhibition (DATE)*, pp. 968–973, 2021.

[16] S. Van Winckel et al., "A 28nm 6.5-8.1ghz 1.16mw/qubit cryo-cmos system-on-chip for superconducting qubit readout," in *ESSCIRC 2022 - IEEE 48th European Solid State Circuits Conference (ESSCIRC)*, to be published, 2022.

[17] A. Caglar et al., "A 4.2mw 4k 6-8ghz cmos lna for superconducting qubit readout," in *2021 IEEE Asian Solid-State Circuits Conference (A-SSCC)*, pp. 1–3, 2021.

[18] G. Burkard et al., "Superconductor–semiconductor hybrid-circuit quantum electrodynamics," *Nature Reviews Physics*, vol. 2, pp. 129–140, jan 2020.

[19] J. van Dijk et al., "A co-design methodology for scalable quantum processors and their classical electronic interface," in *Design, Automation Test in Europe Conference Exhibition (DATE)*, pp. 573–576, 2018.

[20] G. Li et al., "SANQ: A simulation framework for architecting noisy intermediate-scale quantum computing system." arXiv, 10.48550/arXiv.1904.11590, 2019.

[21] D. A. B. Miller, *Quantum Mechanics for Scientists and Engineers*. Cambridge University Press, 2008.

[22] D. Manzano, "A short introduction to the lindblad master equation," *AIP Advances*, vol. 10, feb 2020.

[23] L. Chirolli et al., "Decoherence in solid-state qubits," *Advances in Physics*, vol. 57, pp. 225–285, may 2008.

[24] A. West et al., "Gate-based single-shot readout of spins in silicon," *Nature Nanotechnology*, vol. 14, pp. 437–441, mar 2019.

[25] C. P. Slichter, *Principles of magnetic resonance*. Springer, 3rd ed., 1990.

[26] B. Yurke et al., "Quantum network theory," *Phys. Rev. A*, vol. 29, pp. 1419–1437, Mar 1984.

[27] J. R. Johansson et al., "Qutip 2: A python framework for the dynamics of open quantum systems," *Computer Physics Communications*, vol. 184, no. 4, pp. 1234–1240, 2013.

[28] J.-S. Park, "A fully integrated cryo-cmos soc for qubit control in quantum computers capable of state manipulation, readout and high-speed gate pulsing of spin qubits in intel 22nm ffl finfet technology," in *2021 IEEE International Solid- State Circuits Conference (ISSCC)*, vol. 64, pp. 208–210, 2021.

[29] S. Krinner et al., "Realizing repeated quantum error correction in a distance-three surface code," *Nature*, vol. 605, pp. 669–674, may 2022.

V. Biography

Benjamin Gys obtained his B.Sc. degree in electrical engineering and computer sciences and M.Sc. degree in nanoscience, nanotechnology and nanoengineering from Katholieke Universiteit Leuven, Belgium, in 2018 and 2020 respectively. He is currently pursuing the Ph.D. degree in device architectures and systems for silicon spin quantum computing at the KU Leuven department of electrical engineering and imec Leuven. His research interests include qubit device modelling, cryo-CMOS design and quantum computer microarchitecture design.

Rohith Acharya received his bachelor's degree in electronics and communication engineering from RVCE Bangalore in 2013. Between 2013 and 2016 he worked as a design engineer for Qualcomm Bangalore. He obtained the Erasmus Mundus Master in nanoscience and nanotechnology in the year 2018, jointly from KU Leuven and TU Dresden. Currently he is pursuing his Ph.D. in superconducting qubit design and characterization at the electrical engineering department at KU Leuven and imec Leuven. His research interest includes qubit modelling, design and characterization with an emphasis on low-temperature measurements.

Steven Van Winckel (Member, IEEE) received the master's degree in electrical engineering from the Katholieke Universiteit Leuven, Belgium in 2006. From 2006 to 2008 he joined imec Leuven working in the field of organic semiconductor-based circuit design. From 2008 to 2019 he worked with AnSem Leuven (later acquired by Cyient), on analog, mixed-signal and RF circuit design. From 2019, he rejoined imec Leuven working on cryogenic circuit design and specialty image sensor design.

Kristiaan De Greve is program director quantum computing at imec, part-time professor at KU Leuven (ESAT-MNS) and visiting fellow at Harvard University. He obtained his engineering degree (Burg. Ir. Elektrotechniek, summa cum laude with congratulations of the board of examiners, valedictorian) at KU Leuven - ESAT, with research performed at imec and Caltech. He graduated from Stanford University with a Ph.D. in Electrical Engineering in 2012, where he was a Stanford Graduate Fellow. He was awarded the Springer thesis prize for his Ph.D. research. He joined Harvard University's physics department as a fellow from 2012 until 2019, after which he moved to imec. He holds additional degrees in economics and physics from Stanford, and a mini-MBA from the Harvard Business School. He's the recipient of numerous awards and prizes and has authored multiple patents and over 30 papers in journals like Nature, Science, Nature Physics, Nature Photonics, Nature Nanotechnology, .., which have been highly cited.

Georges Gielen (Fellow, IEEE) received the M.Sc. and Ph.D. degrees in electrical engineering from Katholieke Universiteit (KU) Leuven, Leuven, Belgium, in 1986 and 1990, respectively. He is currently a Full Professor with the Department of Electrical Engineering (ESAT), KU Leuven. His research interests include the design and design automation of analog and mixed-signal integrated circuits. He is a frequently invited speaker/lecturer and a coordinator/partner of several (industrial) research projects in this area, including several European projects. He has authored or coauthored seven books and over 600 papers in edited books, international journals, and conference proceedings. Dr. Gielen was elected as a member of the Academia Europaea in 2018.

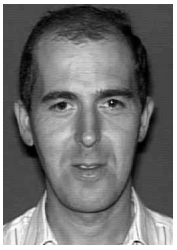

Francky Catthoor received a Ph.D. in EE from the Katholieke Universiteit Leuven, Belgium in 1987. Between 1987 and 2000, he has headed several research domains in the area of synthesis techniques and architectural methodologies. Since 2000 he is strongly involved in other activities at imec including co-exploration of application, computer architecture and deep submicron technology aspects, biomedical systems and IoT sensor nodes, and photo-voltaic modules combined with renewable energy systems, all at imec Leuven, Belgium. Currently he is an imec senior fellow. He is also part-time full professor at the EE department of the KU Leuven. He has been associate editor for several IEEE and ACM journals, and was elected IEEE fellow in 2005.